^{207}Pb and ^{17}O NMR study of the electron density distribution in the metallic phase of BaPb$_{1-x}$Bi$_x$O$_3$

Yu. Piskunov, A. Gerashenko, A. Pogudin, A. Ananyev, K. Mikhalev, K. Okulova, and S. Verkhovskii*
Institute of Metal Physics, UB RAS, Ekaterinburg, Russia

A. Yakubovsky
Russian Research Centre "Kurchatov Institute," Moscow, Russia

A. Trokiner
Laboratoire de Physique du Solide, E.S.P.C.I., Paris, France

The ^{17}O and ^{207}Pb NMR spectra are measured in ceramic samples in the metallic phase of BaPb$_{1-x}$Bi$_x$O$_3$ oxides ($0<x\leqslant0.33$). The inhomogeneous magnetic broadening which appears due to a distribution of the Knight shifts is analyzed in detail. It is shown that Bi atoms, which are randomly incorporated in a BaPbO$_3$ parent compound, give rise to an increased spin density of carriers within an area which is delimited by its two first cation shells. According to NMR data the percolative overlap of these areas occurs in superconducting compositions, and is accompanied by a sharp growth of the average Knight shift $\langle K_s\rangle$. The decrease of $\langle^{17}K_s\rangle$ with temperature revealed for $x=0.33$ evidences that a pseudogap develops near E_F even in a metallic phase near the metal-semiconductor transition ($x_{cr}=0.35$). Our observation supports photoemission results of Uchida *et al.* [Phase Transit. **8**, 95 (1987)] which indicate the opening of pseudogap in superconducting Ba(Pb,Bi)O$_3$ oxides near x_{cr}.

I. INTRODUCTION

During the last two decades many studies have been devoted to the electron states in the conduction band of superconducting BaPb$_{1-x}$Bi$_x$O$_3$ oxides (BPBO). Substituting Bi for Pb in the metallic parent compound, BaPbO$_3$, leads to superconducting compounds in the composition range $0.1<x<0.35$ (Ref. 1) [superconducting composition range (SCR)]. The density of states at Fermi level $N(E_F)$ is found to be small, and T_c, the superconducting transition temperature, estimated from thermal capacity data in the Debye approximation, is substantially smaller than observed T_c.[2–4] According to extended photoemission studies[5–7] a pseudogap near E_F appears for $x\geqslant0.2$, and exists as a real gap for semiconducting compositions ($x>0.35$). Finally, the end member of the family, BaBiO$_3$, is an insulator with an energy gap of ~1 eV due to the commensurate charge density wave (CDW) breathing mode ($\mathbf{qa}=\{\pi;\pi;\pi\}$) developed in the BiO_6-octahedra sublattice. It was considered that electron-phonon coupling might be increased due to the breathing phonon mode existing in the SCR as short-wave charge fluctuations.[8] An exclusively electronic origin of the attractive retarded coupling between the carriers, due to the "skipped valence" effects of Bi, was proposed by Varma,[9] and the relevant phase diagram was developed in Ref. 10 for the semiconducting phase of bismuthates. However, the stability of a uniform electron system in a metallic phase in the presence of a random ionic potential due to cation disorder is still an open question. As noted in Refs. 11–15, changes in the carrier motion near the more electronegative Bi cations can lead to an electronic ground state associated with a non-uniformly distributed electron system in real space.

Most of the experimental data concern parameters describing the electronic and structural properties of an averaged crystal. The static and dynamic effects of the cation disorder in the sublattice of Pb(Bi)O$_6$ octahedra on conduction electrons were considered only in few publications. In discussing neutron-diffraction results, it was concluded[16] that, in the range of $0.12<x<0.3$, the crystal structure of BaPb$_{1-x}$Bi$_x$O$_3$ can be considered as a micro-dispersed mixture of tetragonal and orthorhombic phases. Furthermore, a reversible change of the relative fraction of the two phases occurs with temperature. Extended x-ray-absorption fine structure (EXAFS)[17] and ^{137}Ba NMR and NQR (Ref. 18) studies confirmed the presence of local lattice distortions in the Bi(Pb)O$_6$ sublattice. The influence of short-range ordering of Bi cations in regard to the developed electron instability was studied in Ref. 19. It was shown that some specific configurations of cations give rise to a nonmetallic cluster for metallic compositions $x>0.1$.

Being a local probe of electronic properties, nuclear magnetic resonance is well suited to determining the spatial distribution of electric and magnetic fields of nonhomogeneous structures. The Knight shift $^{207}K_s$ and spin-lattice relaxation rate $^{207}T_1^{-1}$ of lead were measured at $T=4$ K in BaPbO$_3$. The behavior of these properties is similar to that normal metals.[20] ^{17}O (Ref. 21) and ^{207}Pb (Ref. 22) NMR studies showed a monotonic increase of the Knight shift $K_s\sim N(E_F)$ as a function of x when approaching the metal-semiconductor transition, and no evidence of electron correlation effects was reported for a composition $x=0.25$,[22] which corresponds to the highest T_c, $T_{c,max}=12.5$ K. It is worth noting that the aforementioned NMR data were analyzed assuming that all the oxygen and lead ions are located in magnetically equivalent sites of the ideal crystal, ignoring any disorder. Only an abnormally broad distribution of the

^{207}Pb NMR line shift in SCR for $0.10 < x < 0.18$ (Ref. 22) was attributed to the effect of a charge-density-wave (CDW) instability developed in oxides placed compositionally close to the metal-semiconductor transition boundary ($x = 0.35$).

Taking into account these results, we carried out a detailed study of ^{17}O and ^{207}Pb NMR for BaPb$_{1-x}$Bi$_x$O$_3$ in the metallic region ($0 \leq x \leq 0.1$) as well as in the superconducting region ($0.1 \leq x \leq 0.36$). The analysis of NMR spectra shows the formation and evolution of a microscopic inhomogeneous distribution of the charge and spin densities of mobile carriers in these compositions.

II. EXPERIMENT

The measurements were performed on single-phase powder samples BPBO in the range, ($0 \leq x \leq 0.36$). The BPBO samples were prepared with compositions of $x = 0.36, 0.33, 0.27, 0.21, 0.18, 0.15, 0.12, 0.09, 0.03$, and 0. The samples were obtained by a conventional solid-state reaction in air similar to that described in Ref. 23. We put a lot of care into avoiding any macroscopic heterogeneity due to Pb(Bi) substitution. After a preliminary grinding, some of the samples were enriched with the ^{17}O isotope. The powder was poured into a platinum cup, and placed into a quartz tube with flowing ^{17}O$_2$ mounted in the furnace. During the heat treatment the oxygen gas in the quartz loop was continuously scrubbed with Ascarite and cold plate (at 180K). The ^{16}O-^{17}O isotope substitution was carried out at 650 °C for 168 h under an oxygen pressure of 730 Torr. The system was filled twice with "fresh" ^{17}O$_2$. The sample was then cooled to $T = 300$ K with a rate of 15 K/h. According to a mass spectroscopic analysis, the final ^{17}O enrichment of the sample was about 15%. During the preparation and enrichment the cooling rate used was always slow enough to obtain samples with a minimal amount of oxygen vacancies.

The x-ray powder diffraction measurements were performed at $T = 300$ K with a DRON4-A diffractometer with Cu K_α radiation in the range of $2\theta = 10°$-$70°$. To minimize the instrumental error in determining the positions of Bragg reflexes, the sample was mixed with a powder of crystalline germanium. The best fit of the experimental x-ray diffraction patterns was found when assuming an orthorhombic symmetry of the unit-cell parameters for all compositions. No other peaks showing the presence of spurious phases in the samples were revealed. A monotonic decrease of the unit-cell volume is deduced as x increases. The structural parameters of the samples are in a good agreement with the data published in Ref. 24 for BaPb$_{1-x}$Bi$_x$O$_{3-\delta}$ with a small oxygen deficiency, δ.

T_c was determined with ac and dc magnetic susceptibility measurements (Fig. 1). The superconducting transition width does not exceed 2K for $x = 0.25$. The superconducting volume fraction was estimated from the magnetization $M(T)$. It was measured by field cooling (FC) and zero-field-cooling (ZFC) experiments with a SQUID-DESIGN (superconducting-quantum interference device) device operating at $B_0 = 10^{-3}$ T (see the inset in Fig. 1). The deduced Meissner fraction exceeds 0.8 for $x = 0.15$ and $x = 0.27$. For $x > 0.3$ and $x < 0.15$ the superconducting response is absent down to 4K.
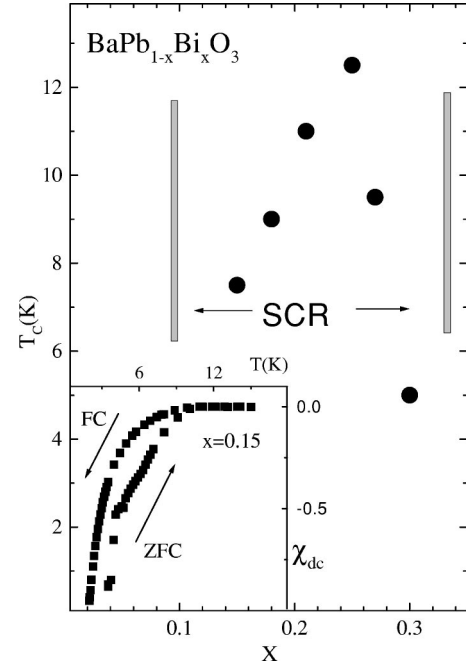

FIG. 1. T_c as a function of x, the bismuth content. The inset shows dc FC and ZFC magnetic susceptibilities vs temperature plots for sample $x = 0.15$. χ_{dc} data are normalized to the susceptibility $\chi_{dc}(2 \text{ K})$ of the Pb sample, having the same form as the measured pellet of the oxide.

Concerning the homogeneity of composition, the x-ray analysis and dc-magnetization data are in favor of a high enough homogeneity on macroscopic scale for all the samples.

^{207}Pb and ^{17}O NMR measurements were carried out on a Bruker NMR pulse spectrometers over the temperature range of 10–350 K in three magnetic fields: 2.0, 9.1, and 11.7 T. The spectra were obtained by a Fourier transformation of the second half of the echo signal obtained with the $(\pi/2)_x - \tau_{del} - (\pi)_x$ pulse sequence. A phase cycling of the pulses was used in order to suppress spurious signals arising from the transient rings in the rf circuit after the pulses. The spectra for which the width exceeds the frequency band excited by the rf pulse were obtained by irradiating the whole spectrum at equidistant frequencies. The spectrum was reconstructed after Fourier transformation of the corresponding echoes.

The components of the magnetic shift tensor (K_{iso}, K_{ax}) for ^{17}O and ^{207}Pb—as well as the electric-field-gradient (EFG) parameters (for ^{17}O) the quadrupole frequency ν_Q and asymmetry parameter η—were determined by a computer simulation of the measured NMR spectra. The powder pattern simulation program takes into account quadrupole coupling corrections up to the second order of the perturbation theory. The NMR powder pattern is calculated with a distribution function of the NMR parameters, and a nonuniform broadening of the spectra can be specified.

For ^{17}O, the positions of the features of both the central line (transition $m = -\frac{1}{2} \leftrightarrow +\frac{1}{2}$) and satellite lines ($m = \pm\frac{1}{2} \leftrightarrow \pm\frac{3}{2}$), were analyzed. We used solid $Pb^{+II}(NO_3)_2$
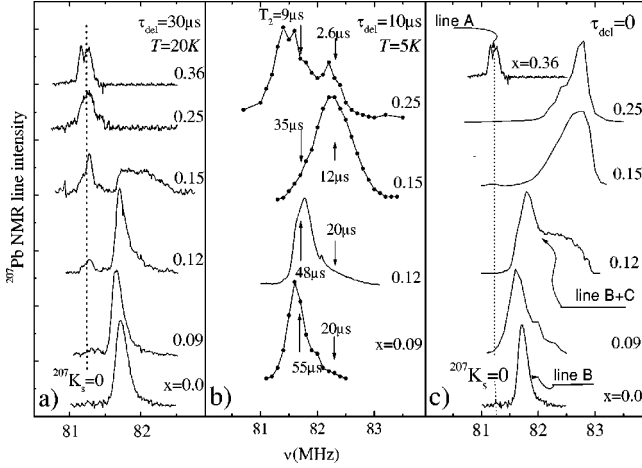
FIG. 2. ^{207}Pb NMR spectra of BaPb$_{1-x}$Bi$_x$O$_3$ measured by the spin echo technique with different delay times τ_{del} between echo pulses.

for ^{207}Pb ($^{207}\nu_L = 80.978$ MHz) and H$_2$O for ^{17}O as frequency references.

Above T_c the magnetic susceptibility χ_m was measured by a Faraday balance technique. The measurements were performed in the temperature range of 4.2–370 K in a magnetic field of 0.5 T, and the instrumental error did not exceed $0.02\chi_m$.

III. EXPERIMENTAL RESULTS AND DISCUSSION

A. ^{207}Pb NMR spectra

The ^{207}Pb NMR spectra shown in Fig. 2 for BPBO samples were obtained at $B_0 = 9.1$ T, in the temperature range of 5–20 K. For SCR, spectra were measured in a normal state, since B_0 exceeds the critical field H_{c2}. A single nonuniformly broadened line (line A) is found at low frequency in the semiconducting region, $x > 0.35$, [Fig. 2(a)]. Its shift $^{207}K(0.36) = 0.30(5)\%$ is in the range of chemical shifts reported for Pb^{+IV} in insulating oxides Ba$_2$PbO$_4$ (0.21%) and Sr$_2$PbO$_4$ (0.23%).[25] Line A still exists in the SCR, but its intensity sharply decreases with decreasing x. For $x = 0.12$ the relative intensity of line A is less than 5% of the total intensity of ^{207}Pb spectrum. Even for $x = 0.36$, less than one-third of the lead atoms contribute to line A [Fig. 2(a)]. Its shift is independent of both T and x. Its spin-lattice-relaxation time T_1 is of order of 1 s, and the spin-spin relaxation time T_2 is about 75(10) μs at $T = 20$ K. At the moment we cannot definitely judge the origin of this line in the SCR. Measurements on semiconducting compositions of BPBO ($0.4 \leqslant x \leqslant 0.9$) are planned to clear up this point.

On the end of the phase diagram, in BaPbO$_3$, a single, nearly Gaussian, symmetric line (line B) is detected at higher frequency (Fig. 2). Its shift, 0.91(2)% is T independent, and is in quite good agreement with published data in Refs. 20–22. As shown in Fig. 2(b), the high-frequency part of the NMR spectra in Bi-containing compounds depends strongly on the delay time τ_{del} between rf pulses. In order to analyze

the spectra obtained in metallic compounds ($x < 0.35$), let us focus on the main features of the $^{207}T_2$ behavior in the high-frequency part of the spectra.

(i) In BaPbO$_3$ the value of $^{207}T_2^{-1}$ greatly exceeds the homonuclear magnetic dipole contribution $^{207}T_{2,dip}^{-1}$ $\approx (0.1-0.3)$ ms^{-1}, estimated for a sample with a natural abundance of lead isotopes. In BaPbO$_3$ and $x = 0.09$ samples, $^{207}T_2(5$ K$) = 55(5)$ μs. In addition, the intensity of the echo, $I(2\tau_{del})$, demonstrates an oscillating behavior at low temperature with $\omega_{osc} = 4.5(5) \times 10^5$ s^{-1}. The homonuclear indirect coupling term $J_{ex}I_{z1}I_{z2}$ is assumed to be responsible for the $^{207}T_2$ in the metallic phase. The exchange integral for BaPbO$_3$ estimated within the Ruderman-Kittel model, $J_{ex} = 0.2 \times 10^{-21}$ erg, was found to be consistent with the measured value of ω_{osc}.

(ii) As shown in Fig. 2(b), $^{207}T_2$ changes within the non-uniformly broadened spectra. The arrows point to the operating frequencies. The data can be fitted with the expression $^{207}T_2(\nu)_{expt}^{-1} \sim {^{207}K_s^\alpha}(\nu)$, where $\alpha = 1.0 - 1.3$ for $x < 0.2$. The Knight shift $^{207}K_s(x)$, for a fixed x, was defined as follows. We have assumed that the chemical part of the total shift does not change with x since the valence state of lead is fixed (Pb^{+IV}). Thus we write

$$^{207}K_s(x) = \{^{207}K(x) - {^{207}K}(x=0.36)\} = \frac{1}{\mu_B}{^{207}H_{hf}}\chi_{s,loc}.$$

(1)

$^{207}H_{hf}$ is hyperfine magnetic field arising due to the hyperfine interaction with conducting electrons, whose spin density near the given atom can be characterized by the local-spin susceptibility $\chi_{s,loc}$.

(iii) The $T_2(\nu)$ values decrease sharply with increasing x on approaching the metal-semiconductor transition.

Taking into account the variation of T_2 within a spectrum, we have restored the real ^{207}Pb NMR line shape in the following way [Fig. 2(c)]: the intensity of echo signals measured at each frequency, ν, with $\tau_{del} = 10$ μs, was multiplied by the factor $\exp[2\tau_{del}/T_2(\nu)]$.

Comparing the restored line shapes ($\tau_{del} = 0$) to the spectra measured with $\tau_{del} = 10$ μs, one may see that line B, corresponding to BaPbO$_3$, is still present in $x = 0.09$ and 0.12 compounds. Nevertheless, the corresponding Knight shift shows a small increase as x increases. Line B is located on a low-frequency edge of a broad line (line C). Line C shifts toward a higher frequency as x increases. On the SCR boundary, for $x = 0.12$, the resulting spectrum has the best resolved structure [Fig. 2(c)] since lines B and C have more or less the same weight. For $x \geqslant 0.15$, mainly line C is present, line B has almost disappeared. The dominant intensity of line C in the SCR corresponds to $^{207}K_s > 1.5\%$.

Thus, substituting Bi in BaPbO$_3$ produces a large broadening of the spectra due to a distribution of the Knight shifts. The broadening is accompanied by a distribution of $^{207}T_2^{-1}(\nu)$ and $^{207}T_1^{-1}(\nu) \sim {^{207}K_s^2}(\nu)$. Both of these quatities are controlled by the Fermi-contact hyperfine interaction with carriers of the conducting band, having local densities of states $N_{loc}(E_F) \sim \chi_{s,loc}$ near a given lead of $^{207}T_2^{-1}(\nu) \sim {^{207}H_{hf}^2}\chi_{s,loc} \sim {^{207}H_{hf}^2}N_{loc}(E_F)$ and $^{207}T_1^{-1}(\nu)$
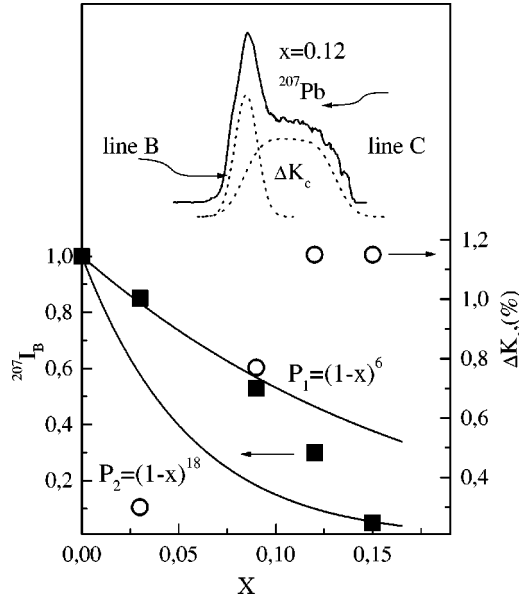
FIG. 3. Relative intensity of the narrow peak $^{207}I_B$ and width line C (ΔK_c) as a function of x in ^{207}Pb NMR spectra of $BaPb_{1-x}Bi_xO_3$.

$\sim {}^{207}H_{hf}^2 [N_{loc}(E_F)]^2$. The ratio $[{}^{207}T_1^{-1}(\nu)]/[{}^{207}T_2^{-1}(\nu)]$ $\sim N_{loc}(E_F)$ is found to increase proportionally ν through a broadened NMR spectrum of ^{207}Pb-like $^{207}K_s(\nu)$. Thus the distribution of $^{207}K_s$ reveals a nonuniform ($q \neq 0$) distribution of the carrier density "depending" on the local environment of the lead atoms.

Let us focus on the nonsuperconducting metallic compounds, $x < 0.12$. Since x is rather small, it is reasonable to assume a random distribution for Bi ions in Pb sites. As shown in Fig. 3, the measured relative intensity of line B ($^{207}I_B$) decreases, while the width of line C ($\Delta K)_C$ increases with increasing x. In parallel, for line C, the relative intensity as well as the shift of the center of gravity [Fig. 2(c)] increases as the Bi concentration increases. Thus Pb atoms located in an area around Bi experience a high local-spin susceptibility $\chi_{s,loc}$. The characteristic radius of this area can be estimated in the assumption of a binomial distribution $P_i(x)$, which is valid only for Bi-diluted oxides. In Fig. 3, the upper curve $P_1(x) = (1-x)^6$ corresponds to the fraction of Pb having no Bi atoms in the nearest cation shell. The bottom curve $P_2(x) = (1-x)^{18}$ is the fraction of Pb having no Bi atoms in both nearest and next-nearest cation shells. The experimental data $^{207}I_B$ are well situated between these two curves, $P_1(x)$ and $P_2(x)$, which means that the radius of the area with high $\chi_{s,loc}$ around Bi, line C being attributed to Pb atoms in these areas, does not exceed 1–2 lattice constants. A steeper decrease of $^{207}I_B$ occurs for $x \gtrsim 0.09$. It is interpreted as due to the percolative overlap of the Bi-containing areas expected for $x \gtrsim 0.12$ near the transition to the SCR

In the SCR, the increase of the relative intensity of line C [Fig. 2(c)] shows that most of Pb nuclei are in the sites with high $\chi_{s,loc}$. ^{207}Pb NMR spectra were available for measurements up to room temperature only for $x \leq 0.15$. It was found that the line position, the total width at half height $(\Delta K_s)_{0.5}$,
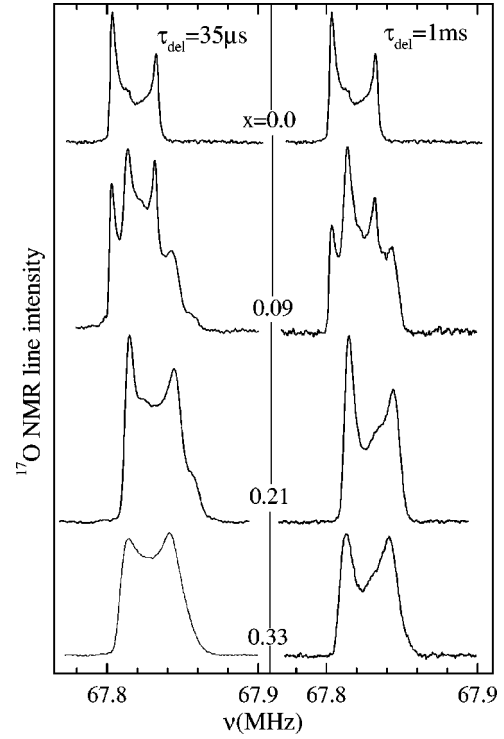

FIG. 4. ^{17}O NMR spectra (transition $m = -\frac{1}{2} \leftrightarrow \frac{1}{2}$) measured at room temperature in $BaPb_{1-x}Bi_xO_3$ by the spin echo technique with different τ_{del}.

and T_2 measured at a given K_s are roughly independent of T. Unfortunately, on the other end of the studied phase diagram, i.e., for $x \leq 0.25$, no echo signal was detected in the range of $^{207}K_s > 0.5\%$, probably due to very short $^{207}T_2 < 1$ μs.

B. ^{17}O NMR spectra

The oxygen atoms are located at the apex of octahedra with Pb or Bi at the centers. The resonance frequency of the ^{17}O NMR probe is determined by both the hyperfine magnetic interaction and the quadrupolar interaction.

The ^{17}O central lines (transition $m_I = -\frac{1}{2} \leftrightarrow +\frac{1}{2}$) measured at room temperature at $B_0 = 12$ T are presented in Fig. 4. The satellite lines corresponding to the transitions $m_I = \pm\frac{1}{2} \leftrightarrow \pm\frac{3}{2}$ were also measured (Fig. 6). A simulation of the central NMR line shapes measured at different magnetic fields allowed us to determine with reasonable accuracy the components $^{17}K_{iso}$ and $^{17}K_{ax}$ of the magnetic shift and the EFG tensors ν_Q and η. ν_Q and η are related to the corresponding Cartesian components V_{ii} of the electric-field gradient:[26]

$$\nu_Q = \frac{3eQV_{ZZ}}{2I(2I-1)h}, \quad \eta = \frac{V_{XX} - V_{YY}}{V_{ZZ}}$$

with

$$|V_{ZZ}| \geq |V_{XX}| \geq |V_{YY}|. \tag{2}$$

For both parent compounds, $BaPbO_3$ and $BaBiO_3$, all the oxygen sites are equivalent since the corresponding spectrum

TABLE I. ^{17}O NMR line parameters (for details see the text and Fig. 5).

		BaPb$_{1-x}$Bi$_x$O$_3$						
	x	0.0	0.03	0.09	0.15	0.21	0.27	0.33
$\dfrac{^{17}K_{iso}}{\delta K_{iso}}$, ppm	line 1			$\dfrac{350(10)}{50(10)}$			–	
	line 2	–				$\dfrac{510(15)}{120(20)}$		
	line 3	–				$\dfrac{700(20)}{250(50)}$		
$^{17}K_{ax}$, ppm	line 1			-40(10)			–	
	line 2	–				-50(10)		
	line 3	–				-70(10)		
$\dfrac{\nu_Q}{\delta\nu_Q}$, MHz	line 1			$\dfrac{1.13(3)}{0.05(3)}$			–	
	line 2	–				$\dfrac{1.15(5)}{0.05(3)}$		
	line 3	–				$\dfrac{1.1(1)}{0.10(5)}$		
η	line 1			<0.05			–	
	line 2	–			<0.05			
	line 3	–	0.05	0.015	0.2	0.3	0.35	0.5
Relative intensity	line 1	1.0	0.81	0.41	0.12		–	
	line 2	0	0.14	0.43	0.69	0.7	0.65	0.6
	line 3	0	0.05	0.16	0.19	0.3	0.35	0.4
$\langle ^{17}K_{iso}\rangle$, ppm	300 K	350(10)	390(10)	480(20)	520(20)	570(20)	580(20)	590(20)
	20 K	350(10)	–	500(20)	–	560(20)	560(20)	500(20)

can be described with a single set of magnetic shift and EFG's. The two-peaked line shape is due to the second-order quadrupole effect on a powder spectrum (see BaPbO$_3$ on Fig. 4). The symmetry of the EFG tensor is almost axial. It should be noted that the values of K_{iso} and ν_Q listed in Table I are consistent with the results reported in Ref. 21.

The magnetic and charge equivalences of the oxygen sites are destroyed in the intermediate metallic compositions, for which spectra show a rather complex structure (Fig. 4), each peak or shoulder having its own dependence on τ_{del} and on the repetition time. The intensity of the high-frequency part of the spectrum grows with increasing x; correspondingly, $(T_2)^{-1}$ is also larger. These changes evidence that in the Bi-containing oxides there is a distribution of the fluctuating hyperfine magnetic fields responsible for processes of spin-lattice and spin-spin relaxations at the oxygen sites.

Less distorted line shapes are obtained for the shortest τ_{del} value, $\tau_{del}=35$ μs$\ll(^{17}T_2)_{min}\approx600$ μs. The powder spectra of the central transition measured at $B_0=12$ T is rather well resolved in the Bi-diluted oxides, $x=0.09$ (Fig. 4). This spectrum is the superposition of three lines, the deconvolution is shown in Fig. 5(a).

All the simulated lines are broadened by convoluting with a Gaussian function. The function is specified in terms of an isotropic shift and quadrupole frequency, and its width at a half of height (δK_{iso}) or/and ($\delta\nu_Q$). The EFG parameters were deduced for each line from the central line measured at low field, $B_0=2$ T (Fig. 5) and the satellite lines (Fig. 6). The calculated spectra are shown by dotted lines in Fig. 5, and the relevant shift and EFG parameters are listed in Table I. For all the metallic compositions the spectra can be simulated with the same three lines, by varying the relative intensities of these lines. Only η was adjusted for line 3 with the

largest magnetic shift. These three lines correspond to three oxygen sites differing mainly in their magnetic hyperfine fields.

In order to understand the origin of the three lines, we have analyzed the variation of the spectra as a function of x. The tensor components of line 1, $^{17}K_{iso}$, $^{17}K_{ax}$, ν_Q, and η are very close to those obtained for pure BaPbO$_3$. Its intensity decreases as the Bi concentration increases. Lines 2 and 3 appear only when Bi cations are present. Considering the measured relative intensities, ^{17}Int$_i(x)$, plotted in Fig. 7, it is quite natural to assume that line 1 originates from oxygen with no Bi in the nearest and next-nearest shells, whereas lines 2 and 3 correspond to oxygen with Bi. Furthermore, the function $(1-x)^{10}$ (Fig. 7, dashed curve), which represents
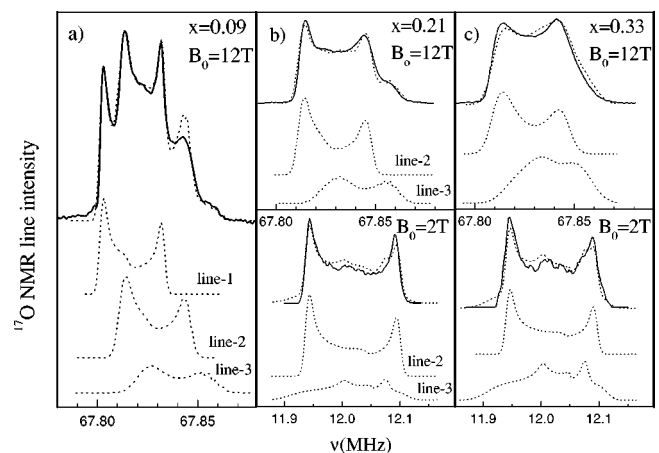

FIG. 5. Experimental and simulated (dotted lines) room temperature ^{17}O NMR spectra (transition $-\frac{1}{2}\leftrightarrow\frac{1}{2}$) in low ($B_0=2$ T) and high ($B_0=12$ T) magnetic fields.

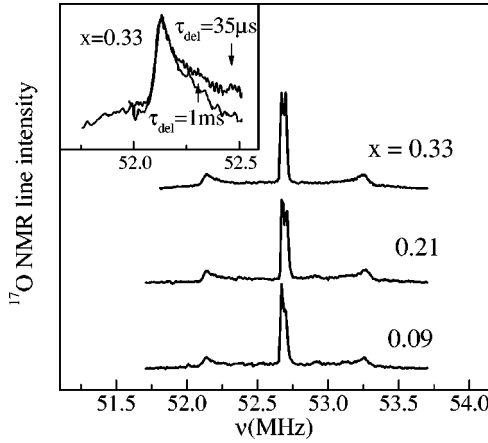FIG. 6. ^{17}O NMR powder patterns for the central line and two first satellites measured in BaPb$_{1-x}$Bi$_x$O$_3$ at room temperature.

FIG. 8. Average Knight shift $\langle^{207}K_s\rangle$ and the electronic thermal capacity coefficient γ_{el} (Ref. 4) vs x in BaPb$_{1-x}$Bi$_x$O$_3$.

the binomial probability of the cation configuration without Bi in both the nearest and the next-nearest cation shells around oxygen, fits ^{17}Int$_1(x)$ very well. Thus line 1 is due to oxygen with no Bi in its two first shells.

The shaded region in Fig. 7 shows the range of the expected relative intensity from the binomial model for different Bi-containing configurations of the first cation shell around a given oxygen. The bottom boundary curve $2x(1-x)$ corresponds to the configuration with a single Bi ion in the nearest cation shell, whereas the top boundary curve $x(2-x)$ relates to the configuration for which one or two Bi ions are present in the nearest cation shell. As seen in Fig. 7, for small x, $x<0.1$, ^{17}Int$_3(x)$ is well described in our model. Thus line 3, with the largest shift, can be attributed to oxygen with at least one Bi as nearest neighbor.

The small deviation of ^{17}Int$_3(x)$ from the binomial predictions for superconducting oxides ($x>0.1$) is believed to originate from the overlapping of the areas with the Bi-stimulated high electron density. In the overlapped areas the Bi-Bi distance is less than two lattice constants, and the foregoing simple binomial approach becomes invalid in the SCR. It should be added that the reduction of the EFG symmetry for line 3 (see η in Table I) favors the suggested assignment.

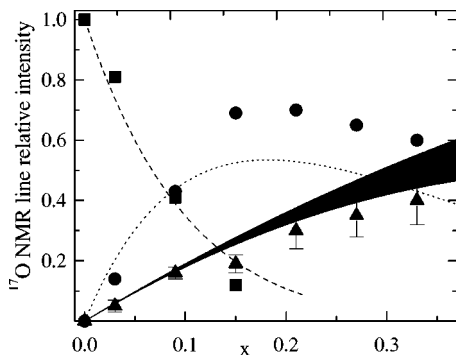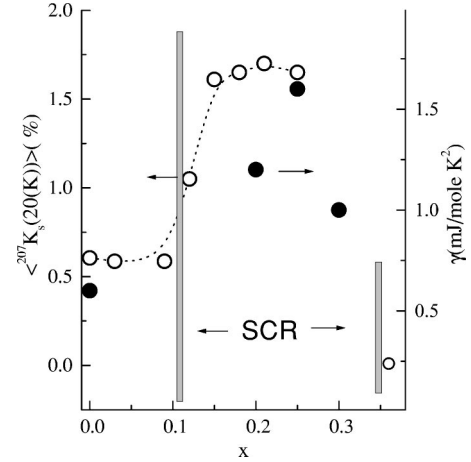Line 2 dominates in the SCR, and its intensity reaches a maximum around $x=x(T_{c,max})$ followed by a monotonic de-

FIG. 7. Relative intensity of the lines, ^{17}Int$_1$, ^{17}Int$_2$ and ^{17}Int$_3$ of the ^{17}O NMR spectra of BaPb$_{1-x}$Bi$_x$O$_3$ as shown in Fig. 5: ■, line 1; ● line 2; ▲, line 3.

crease in going toward the semiconducting compositions. This line might be attributed to oxygen with Bi ions only located in the second cation shell. The probability of this cation configuration, $(1-x)^2[1-(1-x)^8]$, is represented by the dotted line in Fig. 7. As it can be seen, ^{17}Int$_2(x)$ is well described in our model for $x<0.1$.

The increase of the magnetic shift from line 1 to line 3 and the larger $(T_2)^{-1}$ of line 3 have to be put in parallel with the increase of the shift of ^{207}Pb NMR spectra as the Bi content increases [Fig. 2(c)]. As for Pb results, this demonstrates that the random substitution of Pb by Bi in BaPbO$_3$ changes the electron density of carriers within two first cation shells around Bi.

C. Average Knight shift of ^{207}Pb and ^{17}O vs x

The Pb NMR line is broadened and shifted mainly due to the distribution of the Knight shift $^{207}K_s$. The average Knight shift $\langle^{207}K_s\rangle$ is defined as the first moment of the inhomogeneously broadened lines $^{207}g(\nu)$ shown in Fig. 2(c):

$$\langle^{207}K_s\rangle = \frac{\langle \nu - \nu_0(x=0.36)\rangle}{\nu_0(x=0.36)} = \frac{1}{\nu_0}\int (\nu - \nu_0)^{207}g(\nu)d\nu. \tag{3}$$

$\langle^{207}K_s\rangle$ is proportional to the uniform part of the spin susceptibility $\chi_s(q=0)$,[27]

$$\frac{\mu_B\langle^{207}K_s\rangle}{^{207}H_{hf}} = \chi_s(q=0) = \frac{2\mu_B^2 N(E_F)}{1-JN(E_F)}, \tag{4}$$

where $N(E_F)$ is the bare density of states (DOS) at the Fermi level. As seen in Fig. 8, $\langle^{207}K_s\rangle$ sharply increases at the boundary of the SCR. This observation for the average Knight shift $\langle^{207}K_s\rangle$ vs x is in a qualitative agreement with the dependence of the electronic thermal capacity coefficient $\gamma_{el}\sim N(E_F)(1+\lambda)$ on x (Ref. 2). It is instructive to note that γ_{el} probes the bare DOS multiplied by the mass enhancement factor $(1+\lambda)$. The electron-phonon coupling constant was estimated in Ref. 28, and λ was found to increase in
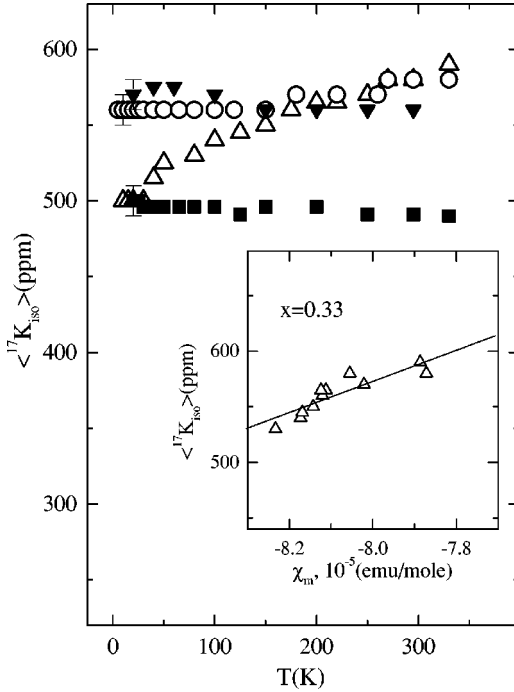
FIG. 9. Temperature dependence of the average NMR shift of oxygen $\langle ^{17}K \rangle$ in BaPb$_{1-x}$Bi$_x$O$_3$: ■, $x=0.09$; ▼, 0.21; ○, -0.27; △, 0.33. The inset shows $\langle ^{17}K \rangle$ vs magnetic susceptibility χ_m of the sample x=0.33.

going toward the SCR. This leads to a more slender x variation of $N(E_F)$ when estimated from the heat capacity data,[2] as compared to the estimation from the Knight shift data. One may assume that ferromagnetic fluctuations in the conduction band increases, and the increase of $\chi_s(q=0)$ occurs due to nonvanishing Stoner's enhancement factor $JN(E_F)$.

Let us now consider the average NMR isotropic shift of oxygen $\langle ^{17}K_{iso} \rangle$. It is defined by an expression similar to Eq. (4), where $^{17}g(\nu)$ is the sum of three Gaussian lines with a relative intensity $(^{17}\text{Int})_i$ and a magnetic shift $(^{17}K_{iso})_i$ corresponding to lines 1, 2, and 3, respectively. The respective widths $(\delta K_{iso})_i$ of the Gaussian lines were deduced from simulation. The thermal behavior of $\langle ^{17}K_{iso} \rangle$ down to $T=20$ K is displayed in Fig. 9. For $x<0.27$, $\langle ^{17}K_{iso} \rangle$ is temperature independent. For $x=0.33$, i.e., near the transition to a semiconducting state, a gradual decrease of $\langle ^{17}K \rangle$ with decreasing temperature is found. For this sample the static magnetic susceptibility is also T dependent. In the range of $T=80$–300 K the measured slope $(\Delta\chi\Delta T)_{x=0.33}=4.5 \times 10^{-11}$ emu/gr K is consistent with the data reported in Ref. 29. Both observations might be interpreted in terms of the pseudo gap phenomenon developing near E_F in superconducting BPBO compositions when approaching the metal-semiconductor transition

The total magnetic shift of ^{17}O NMR line is the sum of two contributions,

$$\langle ^{17}K \rangle(x,T) = \langle ^{17}\delta \rangle(x) + \langle ^{17}K_s \rangle(x,T)$$

$$= \langle ^{17}\delta \rangle + \frac{1}{\mu_B}{}^{17}H_{hf}\chi_s(q=0), \qquad (5)$$

where $^{17}K_s$ is the Knight shift and the other shift contributions are summarized as "the chemical shift" $^{17}\delta$. For light atoms like oxygen both terms in Eq. (5) are comparable in magnitude.

For BaPbO$_3$ we have estimated $^{17}K_s(x=0) = 130(20)$ ppm starting from the ratio of ^{207}Pb and ^{17}O shifts, and using Eqs. (1), (4), and (5). The ratio of corresponding hyperfine fields $(^{207}H_{hf}/^{17}H_{hf})=50(5)$ was estimated by taking into consideration the spin-lattice relaxation rate data of ^{17}O and ^{207}Pb.[21,22,30] The deduced $^{17}\delta$ value is $^{17}\delta(x=0)=220(20)$ ppm. Assuming that $^{207}H_{hf}/^{17}H_{hf}$ is the same in all the metallic samples, we have deduced the x dependence of $\langle ^{17}K_s \rangle$ and $\langle ^{17}\delta \rangle$ using $\langle ^{207}K_s(x) \rangle$ data up to $x=0.25$. We find that $\langle ^{17}\delta \rangle$ is constant within the error bar.

As shown in Sec. III (B) oxygens with no Bi as the nearest neighbor give the main contribution to the ^{17}O NMR line in superconducting samples. Thus one may conclude that no additional paramagnetic (other than χ_{Pauli}) contribution to $^{17}\delta$(line 2) appears at these oxygen sites.

At low temperatures $\langle ^{17}K_s \rangle$ passes through a maximum, and then decreases for $x=0.33$. Assuming that for $x=0.33$ $\langle ^{17}\delta \rangle=200$ ppm, the average Knight shift is about $\langle ^{17}K_s(x=0.33) \rangle=300$ ppm, and the corresponding bare DOS is $N(E_F)_{NMR}=(\langle ^{17}K_s \rangle/2\mu_B{}^{17}H_{hf})=0.16$ (eV spin)$^{-1}$. It should be noted that $N(E_F)_{NMR}$ exceeds more than twice that on $N(E_F)_\gamma$ evaluated from the electronic thermal capacity coefficient γ_{el} in Ref. 29 for $x=0.30$, whose chemical composition is nearly the same as in BaPb$_{0.67}$Bi$_{0.33}$O$_3$.

IV. SUMMARY

The NMR spectra of ^{207}Pb and ^{17}O were measured as functions of temperature and x in the metallic phase and in the superconducting BaPb$_{1-x}$Bi$_x$O$_3$ ($0\leq x\leq0.33$). The magnetic shift and broadening of the spectra were analyzed. It was shown that powder patterns of the spectra are modified due to distribution of the Knight shift. The deconvolution of inhomogeneously broadened spectra by three lines allowed us to reveal a systematic evolution of the separate lines intensities with the Bi concentration. Each of these lines was attributed to a NMR probe with a certain configuration of the neighboring and next-neighboring Pb(Bi) cation shells.

It was established that in Bi-diluted oxides areas with increased density of mobile carriers arise around the Bi atoms. The characteristic size of these areas does not exceed two lattice constants. The percolative overlapping of these areas is expected at higher Bi concentrations in superconducting BPBO compositions. The temperature dependence of magnetic shift for ^{17}O NMR lines gives evidence of the pseudogap phenomenon developed near the Fermi energy in superconducting BPBO oxides near the metal-to-semiconductor transition.

ACKNOWLEDGMENTS

*Corresponding author. FAX: + 7 3432 - 745244. Email address: Verkhovskii@imp.uran.ru

[1] A.W. Sleight, J.L. Gilson, and P.E. Bierstadt, Solid State Commun. **17**, 27 (1975).

[2] B. Batlogg, Physica B **126**, 275 (1984), and references therein.

[3] S. Uchida, K. Kitazawa, and S. Tanaka, Phase Transit. **8**, 95 (1987).

[4] T. Itoh, K. Kitazawa, and S. Tanaka, J. Phys. Soc. Jpn. **53**, 2668 (1984).

[5] H. Namatame, A. Fujimori, H. Takagi, S. Uchida, F.M.F. de Groot, and J.C. Fuggle, Phys. Rev. B **48**, 16 917 (1993).

[6] H. Sakamoto, H. Namatame, T. Mori, K. Kitazawa, S. Tanaka, and S. Suga, J. Phys. Soc. Jpn. **56**, 365 (1987).

[7] S. Tajima, S. Uchida, A. Masaki, H. Takagi, K. Kitazawa, S. Tanaka, and S. Sugai, Phys. Rev. B **35**, 696 (1987).

[8] K. Machida, Physica C **156**, 276 (1988).

[9] C.M. Varma, Phys. Rev. Lett. **61**, 2713 (1989).

[10] A. Taraphder, H.R. Krishnamurthy, R. Pandit, and T.V. Ramakrishnan, Phys. Rev. B **52**, 1368 (1995).

[11] S. Sugai, Solid State Commun. **72**, 1187 (1989).

[12] T.M. Rice and L. Sneddon, Phys. Rev. Lett. **47**, 689 (1981); Physica B & C **107**, 661 (1981).

[13] M. Suzuki and T. Murakami, Solid State Commun. **53**, 691 (1985).

[14] M. Nagoshi, T. Suzuki, Y. Fukuda, A. Tokiwa-Yamamoto, Y. Syono, and M. Tachiki, Phys. Rev. B **47**, 5196 (1993).

[15] N. Anshukova, A. Golovashkin, L. Ivanova, O. Maljuchkov, and A. Rusakov, Zh. Éksp. Teor. Fiz. **106**, 2132 (1995) [JETP **106**, 2132 (1995)].

[16] D.T. Marx, P.G. Radaelli, J.D. Jorgensen, R.L. Hitterman, D.G. Hinks, S. Pei, and B. Dabrowski, Phys. Rev. B **46**, 1144 (1992).

[17] A.P. Menushenkov, S. Benazeth, J. Purans, A. Ignatov, and K.V. Klementev, Physica C **277**, 257 (1997).

[18] K. Kumagai *et al.*, Physica C **274**, 209 (1997).

[19] U. Hahn, G. Vielsack, and W. Weber, Phys. Rev. B **49**, 15 936 (1994).

[20] T. Tsuda, H. Yasuoka, and R. Remeika, J. Phys. Soc. Jpn. **56**, 3032 (1988).

[21] L. Reven, J. Shore, S. Yang, T. Duncan, D. Schwartz, J. Chung, and E. Oldfield, Phys. Rev. B **43**, 10 466 (1991); E. Oldfield, Ch. Coretsopoulos, S. Yang, L. Reven, H.Ch. Lee, J. Shore, O.H. Han, E. Ramli, and D. Hinks, *ibid.* **40**, 6832 (1989).

[22] F.J.M. Benschop, H.B. Brom, H.W. Zandbergen, and R.J. Cava, Physica C **235-240**, 2527 (1994).

[23] T. Hashimoto and H. Kawazoe, Solid State Commun. **87**, 251 (1993).

[24] T. Hashimoto *et al.*, Physica C **246**, 228 (1995).

[25] A. Gerster, Diplomarbeit, 2. Phys. Institut, Universitaet Stuttgart, 1994.

[26] A. Abragam, *The Principles of Nuclear Magnetism*, (Clarendon Press, Oxford, 1961).

[27] A. Narath, in *Hyperfine Interactions*, edited by A.J. Freeman and R.B. Frankel (Academic Press, New York, 1967).

[28] V. Bogatko and Yu.N. Venevtsev, Fiz. Tverd. Tela (Leningrad) **22**, 1211 (1980) [Sov. Phys. Solid State **22**, 705 (1980)].

[29] S. Uchida, H. Hasegawa, K. Kitazawa, and S. Tanaka, Physica C **156**, 157 (1988).

[30] Yu. Piskunov *et al.*, in *Proceedings of XXXI Russian Conference on Low Temperature Physics, Moscow, 1998* (unpublished).